ACS OMEGA

http://pubs.acs.org/journal/acsodf

Article

Synthesis, Characterization, and Antimicrobial and Nematicidal Activities of Chitosan-Based Silver-Doped Titanium Dioxide

Muhammad Usman Khan, Wajid Rehman,* Saira Bibi, Mohammed M. Alanazi, Ashwag S. Alanazi, Liaqat Rasheed, Shoaib Khan, Syed Umar Tariq Gillani, and Arslan Tauqeer

Cite This: *ACS Omega* 2023, 8, 19341−19350

Read Online

ACCESS | Metrics & More | Article Recommendations

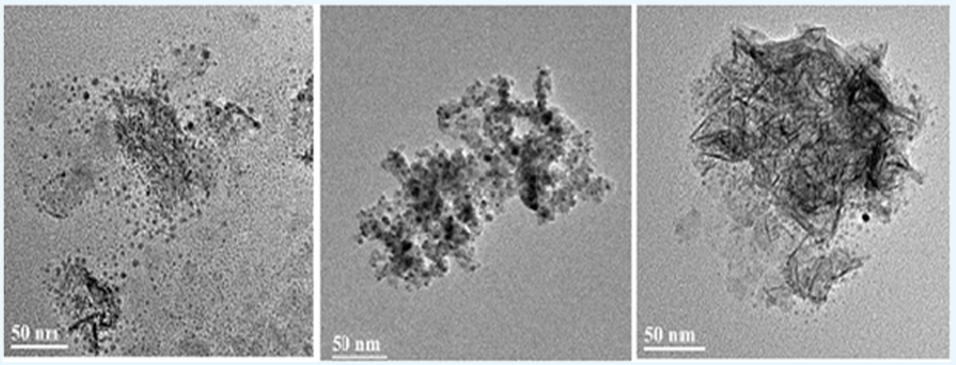

ABSTRACT: Chitosan (Cs)-based silver-doped titanium dioxide (Cs-$AgTiO_2$) films were synthesized intending their end-use application in food packaging. $AgTiO_2$ NPs were successfully prepared by using electrochemical synthesis. Cs-$AgTiO_2$ films were synthesized by using the solution casting technique. Various advanced instrumental techniques such as scanning electron microscopy (SEM), X-ray diffraction analysis (XRD), transmission electron microscopy (TEM), and Fourier transform infrared spectroscopy (FT-IR) were used for the characterization of Cs-$AgTiO_2$ films. Intending their food packaging applications, samples were further investigated to obtain varied biological results including antibacterial (*Escherichia coli*), antifungal (*Candida albicans*), and nematicidal activities. *Ampicillin* (*E. coli*) and *fluconazole* (*C. albicans*) were used as models. FT-IR and XRD confirm the structural modification of Cs. IR peak shifting was observed, which confirmed that $AgTiO_2$ interacted with chitosan via amide I and amide II groups. This confirmed the stability of the filler in the polymer matrix. SEM also confirmed the successful incorporation of $AgTiO_2$ NPs. Cs-$AgTiO_2$ (3%) shows excellent antibacterial (16.51 ± 2.10 μg/mL) and antifungal (15.67 ± 2.14 μg/mL) activities. Nematicidal assays were also done, and *Caenorhabditis elegans* (*C. elegans*) was used as a model organism. Cs-$AgTiO_2$ NPs (3%) exhibited excellent nematicidal potential (64.20 ± 1.23 μg/mL), which could make these films a suitable novel material to control nematode spread in food.

1. INTRODUCTION

Food packaging with health-related information has recently caught the interest of many individuals. On the other side, the plastic polymers being used in the current packaging of foods are non-biodegradable and petroleum-based with a harmful impact on the marine environment. Contrarily, the majority of food packaging is not able to preserve the quality of ingredients in the absence of an aseptic entity, which itself is harmful to one's health. The creation of a biodegradable, microbial-resistant, and inexpensive polymer film is crucial when it comes to the packaging of food as a result.[1]

The packaging material seeks traits including ease of use, biodegradability, renewability, and accessibility within the municipal solid waste; however sadly, researchers have not yet discovered another material exhibiting these characteristics. Furthermore, each material used to package food has a unique combination of benefits and drawbacks that are not exhaustive.

Since glass possesses excellent barrier, transparent, and inert qualities, it is likely the best choice of material for packaging when it comes to food. In addition, it suffers due to its weight, restricted movement, and fragility. However, because of their weight, metal sheets, as well as metal, become less opaque and portable and more inert than glass, which give them a

Received: January 4, 2023
Accepted: May 11, 2023
Published: May 23, 2023

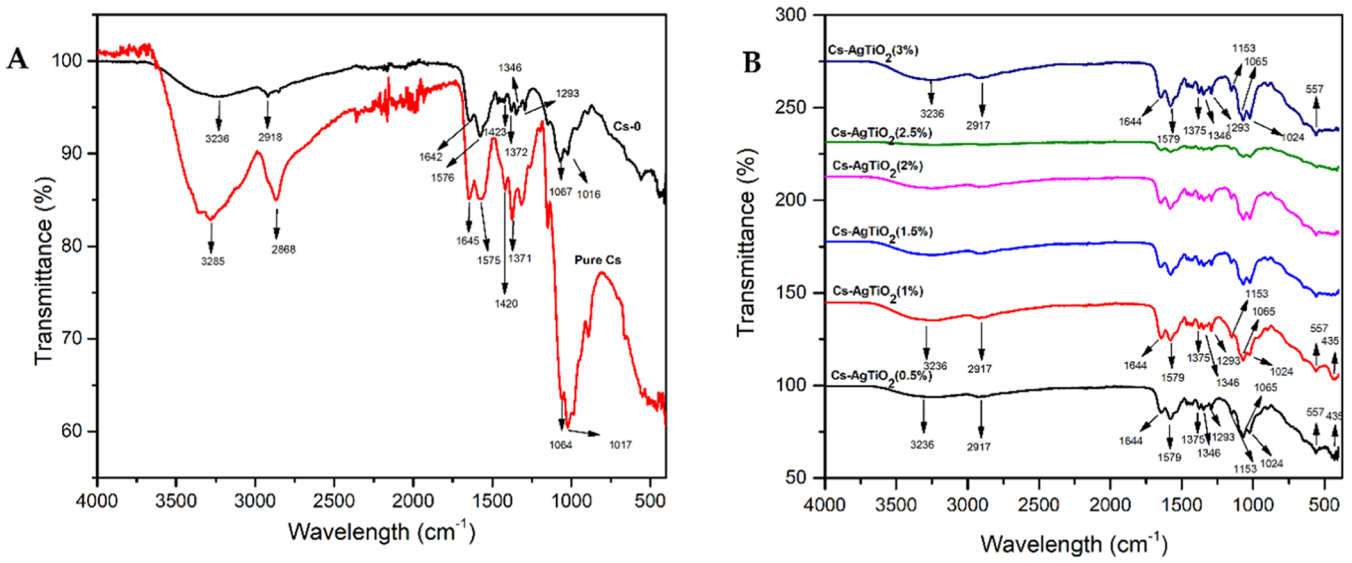

Figure 1. FTIR spectra of (A) Cs/PVA blend (Cs-0) and (B) Cs with different concentrations of $AgTiO_2$.

competitive advantage over glass. It is also advantageous throughout this case to use affordable, flexible, and inert papers and plastics. Plastics also have tensile as well as strong barrier properties and are lightweight and transparent.[2]

The most well-known but also popular materials for packaging food are plastic as well as polymers. The applications for these materials that are neither flexible nor rigid packaging are numerous. In contrast, a US analysis found that plastics cannot decompose naturally. As stated by the EPA, plastics generated MSW in 2014, which is worth taking into account. 32.29 MT of plastic trash, approximately 12.90% of the total amount of municipal waste produced during 2014 (258 MT of MSW), was produced (MSW). 14.32 MT of plastic waste from packaging, representing 43% of the total plastic waste, was produced.

The development producing MSW has become a significant environmental problem in recent years due to the prevalence of plastics throughout the packaging of food. These have inspired research toward biopolymers, which are not only biodegradable but also possess antioxidant as well as antibacterial properties, prolonging the shelf life of food goods. Polymers that are biodegradable including PVA as well as chitosan exhibit biocompatibility, and their formation of a good film has drawn a large amount of interest because of their advantages for the environment.[3]

Cs is the substance most frequently used in the coating and film sectors. Due to its film forming ability, biodegradability, antibacterial activity, and biocompatibility, it is viewed as a viable choice for food packaging.[4] By improving the extraction technique but rather altering the deacetylation process, Cs is however extremely flexible, allowing for the development of alternative materials and thus the demonstration of unique functional abilities. The development of novel materials for food packaging might result from the blending of bioactive chemicals possessing film forming properties with biopolymers.[5] Natural ingredients can facilitate packaging with antibacterial as well as antioxidant qualities, providing those innovative formulations with more effective substitutes for the synthetic preservatives which have been frequently employed with foods.[6]

TiO_2 and $AgTiO_2$ NPs have received a lot of focus recently because of their distinct electrical, chemical, and optical properties. Due to its excellent photocatalytic properties, high efficiency, potent oxidizing capability, chemical stability, benign makeup, and relative affordability, TiO_2 is a fantastic photocatalyst that is frequently utilized for antibacterial activity.[7] The antibacterial property of TiO_2 is crucial, while it is also a promising photocatalyst. Accordingly, it is ecologically beneficial, extremely catalytic, biocompatible, and inexpensive.[8,9] Numerous interdisciplinary studies have been conducted on TiO_2 to improve the photocatalytic activity.[10−12] The doping, hydroxyl group, surface area, and crystalline structure of NPs are all known to affect their photocatalytic activity. Presently, numerous researchers are working to increase the effectiveness of photocatalysts by utilizing metal dopants, such as Ag, which is the most efficient because of its thermal conductivity/good electrical and high stability. Additionally, by slowing down fast e^-−h^+ recombination processes, Ag doping on the surface of metal oxides is used to increase the photocatalytic activity. This method may potentially result in the development of strong antibacterial characteristics.[13−15]

Consequently, both synthetic and natural polymers can have a variety of advantageous properties. However, new polymer materials with the best thermal and mechanical properties for a range of applications can be generated by blending or combining components. These polymers can also be made to be biocompatible and biodegradable. They are used to modify the polymer's properties and function well as additives.[16,17] Cs has undergone different modifications for a variety of uses, including crosslinking, grafting, functionalization, inserting nanofillers, and merging with other polymers.[17−20] Islam et al. showed that the stability and mechanical strength of the material were enhanced by the addition of polyvinyl alcohol and TEOS crosslinking.[19]

In this study, Cs-$AgTiO_2$ was developed on Ag and TiO_2 metal for the first time in the literature, intending to enhance antibacterial and nematicidal capabilities. The solution casting method was applied to prepare the targeted material for the biological system. The surface morphologies, phase structure, functional group, and all the attributes were examined via SEM, XRD, and Fourier transform infrared spectroscopy (FTIR). Additionally, Gram-negative (*Escherichia coli*) bacteria were tested and evaluated for their in vitro bioactivity under physiological settings and antibacterial qualities.

https://doi.org/10.1021/acsomega.3c00068
ACS Omega 2023, 8, 19341−19350

2. RESULTS AND DISCUSSION

2.1. Fourier Transform Infrared (FT-IR) Spectroscopy. In order to identify the functional groups of the synthesized samples, FT-IR spectroscopy was performed. The study was also performed for pure commercial chitosan that was used throughout the preparation of other samples.[21] From the FT-IR spectra, the Cs spectrum shows its distinctive absorption bands at 1576 cm^{-1} (−NH2 bending), 1642 cm^{-1} (amide I), and 1371 cm^{-1} (amide III). The adsorption band at 1018 and 892 cm^{-1} represents the skeletal vibrations involving the C−O−C stretching, which are characteristics of the saccharine structure.[22] In the same image, the blend of Cs/PVA (Cs-0) showed the peaks at 3236 cm^{-1} concerned with overlapping −OH and −NH stretching vibration width and shifting the peak. It was because of the addition of PVA, representing the formation of hydrogen bonding between Cs and PVA, while the peaks at 2918 cm^{-1} and around indicate the crosslinker, which formed between amino groups of chitosan and around aliphatic C−H stretching. In Figure 1B, FT-IR spectra conformed to the overlying of numerous peaks, having a different content of $AgTiO_2$ in Cs.[23] In addition, another strong peak at 1642 and 1645 cm^{-1} (Figure 1B) corresponds to the formation of an amine bond (C = N), which is directly related to the Cs.[24,25] The peaks at 1576 cm^{-1} (1579 cm^{-1}/Figure 1B) show symmetric deformations of the $NH3^+$ group as a result of ionization of primary amine groups in PVA, whereas 1420 cm^{-1} refers to the carboxylic acid that represents the poly(vinyl alcohol) content. The strong peaks at 1371 cm^{-1} are related to the −CH vibration, whereas in Figure 1B, 1375 cm^{-1} corresponds to the N−O group. On the other hand, 1064 cm^{-1} refers to the peaks of chitosan. The intense peak at 806 cm^{-1} chastely corresponds to the Ag−O in Figure 1B. Similarly, the peaks at 2400, 1157, 557, and 451 cm^{-1} characterize the presence of Ag−O, AgNO2, Ti−O, and Ag−O, respectively. The pure $AgTiO_2$ values are in accordance with values reported in the literature.[26] IR peak shifting was observed, which confirmed that $AgTiO_2$ interacted with chitosan via amide I and amide II groups. This confirmed the stability of the filler in the polymer matrix.

2.2. X-ray Diffraction Analysis (XRD). The XRD patterns of Cs-$AgTiO_2$ at different concentrations of $AgTiO_2$ (0.5−3%) are shown in Figure 2. The XRD data were obtained via X'pert high-score software shown in Table 1. The XRD pattern revealed a reflection at 2 = 13.27° (JCPDS Card Number 00-026-1777), which corresponds to the characteristics of Cs. Previously, Kumar and co-authors also reported the same reflection peak. The peak described above is weak in all samples after the addition of nanoparticles. This revealed the successful inclusion of nanoparticles in Cs films. The crystallite size of chitosan was measured by using the Scherrer calculator, which comes out to be 0.1 nm, and the lattice strain is 2.152%.[27]

The XRD patterns of TiO and AgO were observed at 2θ values of 29.46 and 42.050°, respectively. Their corresponding reflection planes are 111 and 222, respectively. The crystal systems of TiO_2 and AgO were found to be monoclinic and tetragonal (JCPDS cards numbers 00-046-1237 and 01-084-1108, respectively). The crystalline sizes of TiO and AgO were 304.6 and 118.2 nm and their lattice strains were 0.044 and 0.080%, respectively.[28]

Furthermore, in all the Cs-$AgTiO_2$ samples, major 2θ peak positions of the diffraction pattern could be shown to have no planes other than the intensities of these peaks shifting. Due to Ag doping, the phases of TiO_2 NPs remained unchanged.

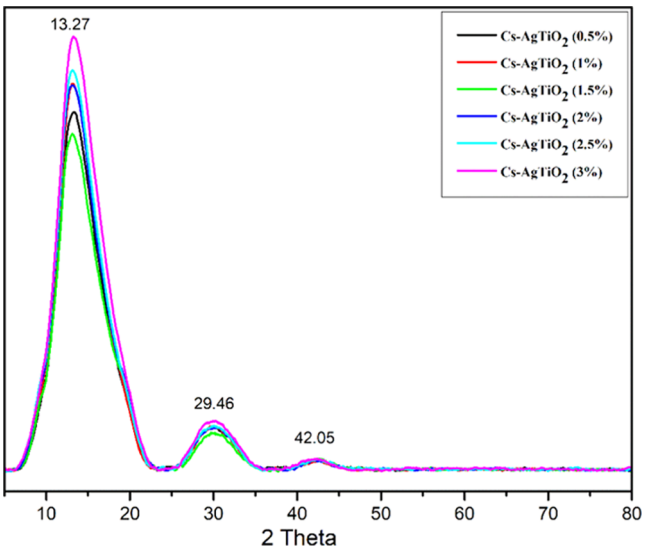

Figure 2. XRD patterns of Cs-$AgTiO_2$.

Table 1. XRD Analysis of Cs-$AgTiO_2$

position 2θ	*d*-spacing	FWHM	$(h + k^2 + l^2)$	*h k l*
13.27°	6.51000	0.5702		
29.46°	2.98164	0.0269	3	1 1 1
42.05°	2.14702	0.0720	12	2 2 2

Because the Ag^+ ion radii (126) were too large to completely replace the Ti^{4+} (68) ions in the TiO_2 matrix, it was demonstrated that Cs-$AgTiO_2$ is homogeneously distributed and that there has been no appreciable change in the crystallinity of TiO_2. Therefore, the addition of Ag did not alter the TiO_2 phase structure, indicating that Ag was generated on the crystal grain boundary and the surface of the TiO_2.[29]

2.3. Scanning Electron Microscopy (SEM). The surface morphology of the Cs-based Ag-doped TiO_2 films of different weight percents (0.5, 01, 1.5, 02, 2.5, 03%) of $AgTiO_2$ nanoparticles was studied with the help of scanning electron microscopy as shown in Figure 3. The Cs-$AgTiO_2$ nanoparticles, many chunks, and aggregates were randomly dispersed on the top layer of membranes rather than a uniform coating, particularly in the case of high concentration of nanoparticles, and a similar pattern was observed by Zhang et al.[30] These larger particles might be the result of the agglomeration of smaller particles primarily due to the accumulation of Cs-$AgTiO_2$ nanoparticles.[31]

2.4. Transmission Electron Microscopy. To support the surface morphology of Cs-based Ag-doped TiO_2 films, the $AgTiO_2$ was checked through TEM (Figure 4); TEM images were provided for three concentrations (1, 2, and 3%). The images at all three concentrations reveal silver nanoparticles with various small sizes. It is worthy to notice that some dark parts in images may be due to the large number of Ag^0 (metallic silver), which increases with the increase of TiO_2 concentration, and it confirms the adsorption of Ag^0 nanoparticles on titania.

2.5. Antibacterial Activity of Cs-$AgTiO_2$. Antibacterial activity of different concentrations of $AgTiO_2$ (0.5−3%) was investigated against *E. Coli*. GNB (*E. Coli*) was treated with 0.5, 1, 1.5, 2, 2.5, and 3%.[32] *Ampicillin* (*E. Coli*) was used as a model organism. The zone of inhibition in the cases of 0.5−2% against *E. coli* was 9.12 ± 1.1214, 10.31 ± 1.2114, 11.25 ± 2.1214, and 12.23 ± 1.2314 μg/mL. Therefore, 2.5 and 3% show the highest

https://doi.org/10.1021/acsomega.3c00068
ACS Omega 2023, 8, 19341−19350

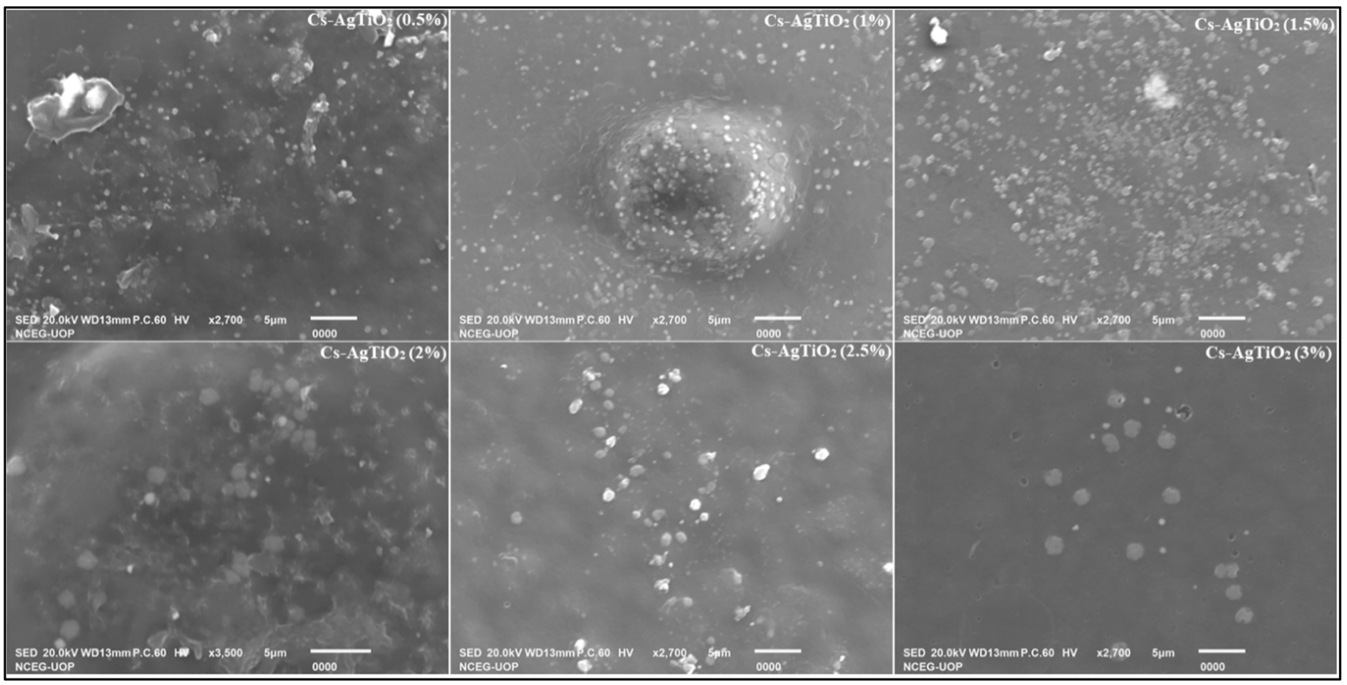

Figure 3. SEM images of Cs-AgTiO$_2$ at different concentrations.

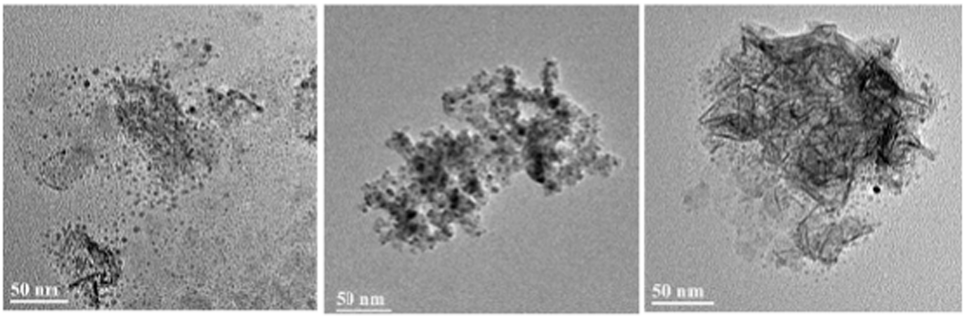

Figure 4. TEM images of Cs-AgTiO$_2$ at different concentrations.

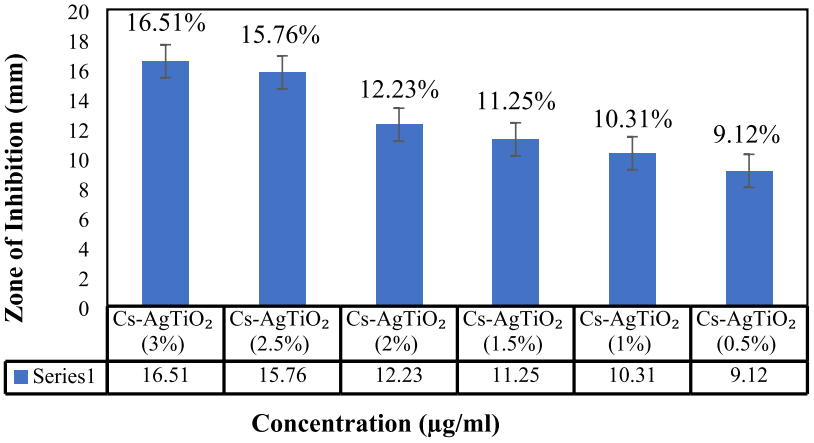

Figure 5. Maximum zone of inhibition of different concentrations of Cs-AgTiO$_2$.

zones of inhibition against *E. Coli* 15.76 ± 1.20 and 16.51 ± 2.10 μg/mL as shown in Figures 5 and 6, respectively. Table 2 shows that the antibacterial activity increases as the concentration of AgTiO$_2$ increases. Figure 5 shows an overview of the antibacterial growth of the Cs-AgTiO$_2$ that was utilized as a positive control.[33]

2.6. Antifungal Activity of Cs-AgTiO$_2$. Antifungal activity was determined by measuring the inhibitory zone. The synthesized Cs-AgTiO$_2$ films at different concentrations of AgTiO$_2$ (0.5, 1, 1.5, 2, 2.5, 3%) were treated against *Candida Albicans*.[34] *C. Albicans* was used as a model organism. The maximum zone of inhibition was 15.67 ± 2.14 μg/mL, present in

https://doi.org/10.1021/acsomega.3c00068
ACS Omega 2023, 8, 19341−19350

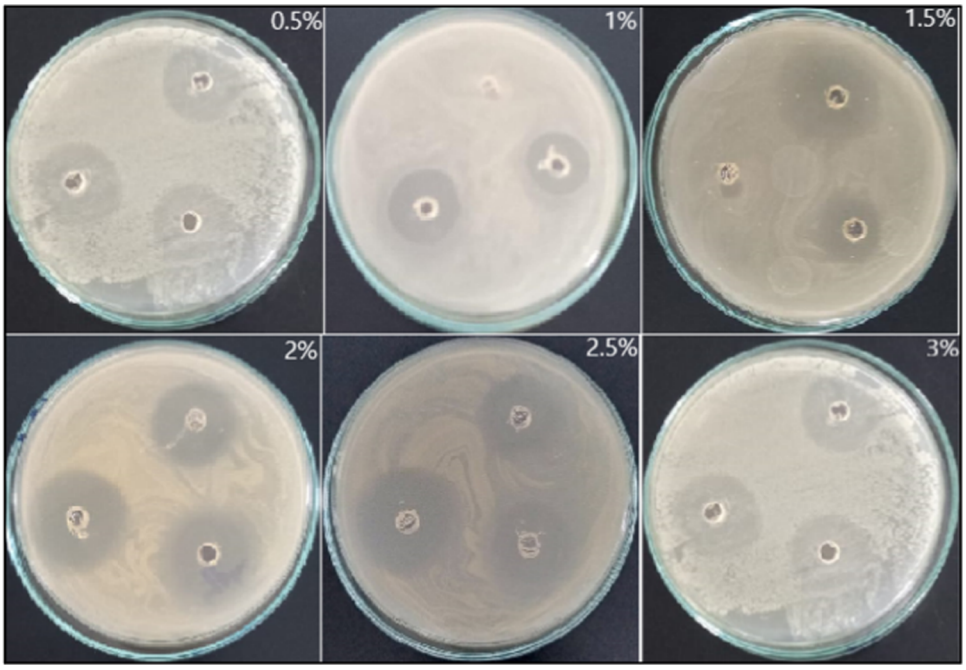

Figure 6. Antibacterial activity of Cs-$AgTiO_2$ at different concentrations.

Table 2. Antibacterial Activity of Different Concentrations of Cs-$AgTiO_2$

		zone of inhibition (mm)		
s. no	reference materials	50 μg	100 μg	150 μg
E. coli	Cs-$AgTiO_2$ (0.5%)	5.10 ± 1.23	7.67 ± 1.41	9.12 ± 1.12
	Cs-$AgTiO_2$ (1%)	6.23 ± 1.31	8.43 ± 1.23	10.31 ± 1.21
	Cs-$AgTiO_2$ (1.5%)	7.14 ± 1.20	9.26 ± 2.14	11.25 ± 2.12
	Cs-$AgTiO_2$ (02%)	9.16 ± 1.26	11.17 ± 2.30	12.23 ± 1.23
	Cs-$AgTiO_2$ (2.5%)	10.74 ± 2.13	13.35 ± 1.34	15.76 ± 1.20
	Cs-$AgTiO_2$ (03%)	12.56 ± 2.15	14.54 ± 2.20	16.51 ± 2.10

Table 3. Fungal Culture of Different Concentrations of Cs-$AgTiO_2$

		zone of inhibition (mm)		
s. no	reference materials	50 μg	100 μg	150 μg
Candida Albicans	Cs-$AgTiO_2$ (0.5%)	4.63 ± 1.12	6.78 ± 1.13	7.60 ± 1.26
	Cs-$AgTiO_2$ (01%)	5.25 ± 1.30	7.51 ± 1.34	9.32 ± 1.31
	Cs-$AgTiO_2$ (1.5%)	7.61 ± 1.21	8.34 ± 1.20	10.21 ± 1.19
	Cs-$AgTiO_2$ (02%)	8.42 ± 2.13	9.56 ± 2.34	11.38 ± 2.13
	Cs-$AgTiO_2$ (2.5%)	9.21 ± 1.31	11.70 ± 2.21	13.23 ± 1.16
	Cs-$AgTiO_2$ (03%)	11.30 ± 2.14	12.13 ± 1.14	15.67 ± 2.14

the case of 3%. However, the cases of 2.5, 2, 1.5, 1, and 0.5% show inhibitory zones of 13.23 ± 1.16, 10.38 ± 2.13, 10.21 ± 1.19, 9.32 ± 1.31, and 7.60 ± 1.26 μg/mL against *C. Albicans*, respectively, as shown in Table 3. Figures 7 and 8 show that as the concentration of $AgTiO_2$ increases, the antifungal activity increases; both are directly proportional to each other.[35]

2.7. Antinematode Activity of $AgTiO_2$. The antinematode activity of the synthesized Cs with different concentrations of $AgTiO_2$ (0.5, 01, 1.5, 02, 2.5, and 03%) was examined. As a food source, *C. elegans* was transported along with *E. coli*. Nematode detection was carried out using 96-well plates. *Caenorhabditis elegans* (*C. elegans*) was used as a model organism. The presence of worms was confirmed using a microscope after adding *C. elegans* to each well at 40−60 and maintaining the plates at 20 °C for 24 h.[36]

At a concentration of 80 μg/mL compounds (3, 2.5, 2, 1.5, 1, 0.5%), $AgTiO_2$ shows potential results against worms and killed 64.20 ± 1.2322, 52.02 ± 2.3542, 44.54 ± 0.5362, 31.12 ± 3.2622, 26.45 ± 1.2653, and 20.65 ± 1.2653 μg/mL *C. elegans*, respectively, as shown in Figure 9.[37]

2.8. Tensile Strength of Cs-$AgTiO_2$. Mechanical properties of the materials are very important parameters to analyze the selectivity for the packaging of the food materials. The tensile strength of the Cs-$AgTiO_2$ varied in compositions and showed 33.1−123.5 MPa of the films and Cs-$AgTiO_2$ (3%) film to be more stable than the other ones (Figure 10).

2.9. Cytotoxicity through Brine Shrimp Lethality. In this, cytotoxicity of the films was up to 50 percent of the lethality concentration. It has been shown that the early stages of *Artemia salina* are encouraging to toxins. Hence, it is concluded that a

https://doi.org/10.1021/acsomega.3c00068
ACS Omega 2023, 8, 19341−19350

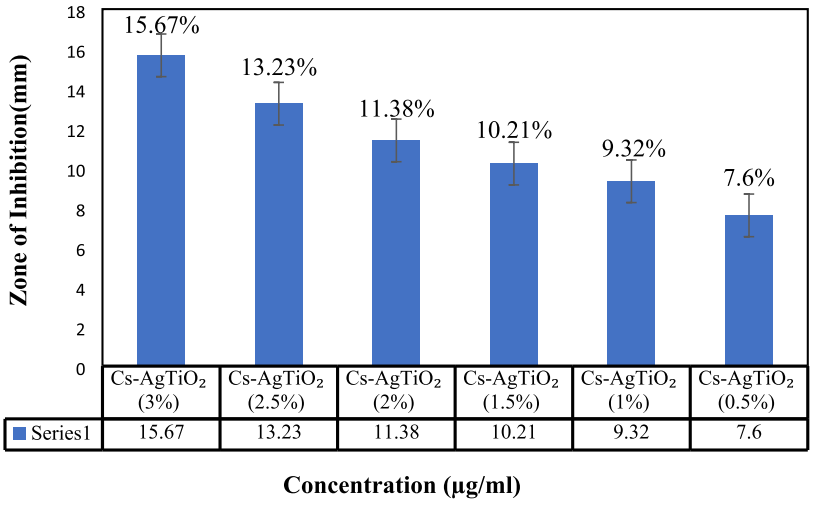

Figure 7. Inhibitory zone at different concentrations of Cs-$AgTiO_2$.

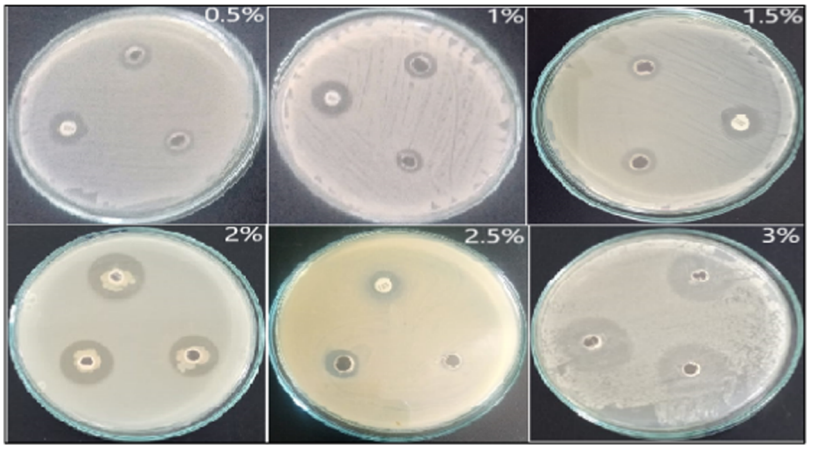

Figure 8. Antifungal activity of Cs-$AgTiO_2$ at different concentrations.

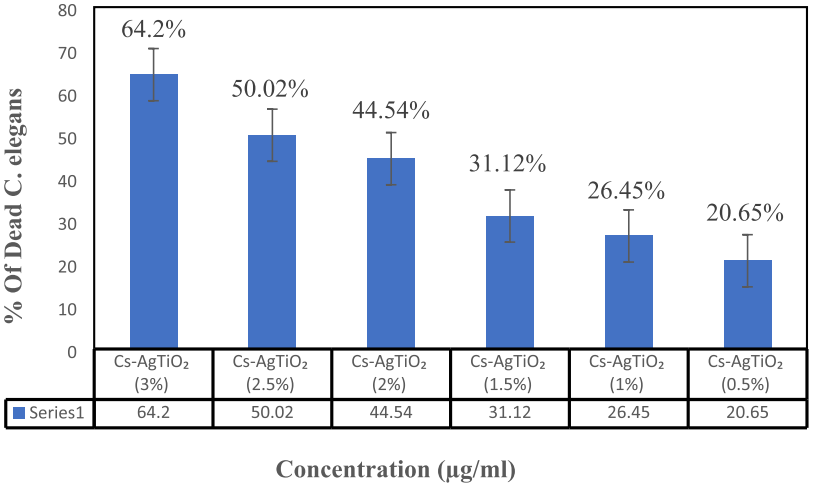

Figure 9. Effect of Cs-$AgTiO_2$ at different concentrations on *C. elegans*.

higher death rate occurs at the higher concentration, which means that these films have lower toxicity (Table 4).[38]

3. CONCLUSIONS

Cs-$AgTiO_2$ films were synthesized by using the solution casting technique. FTIR and XRD confirm the structural modification of Cs. SEM also confirmed the successful incorporation of $AgTiO_2$ NPs. *E. coli* (*ampicillin*) and *Candida albicans* (*fluconazole*) were used as model organisms. Cs-$AgTiO_2$ (3%) shows excellent antibacterial (16.51 ± 2.10 μg/mL) and antifungal (15.67 ± 2.14 μg/mL) activity. Nematicidal assays were also done, and *C. elegans* was used as a model organism. Cs-

https://doi.org/10.1021/acsomega.3c00068
ACS Omega 2023, 8, 19341−19350

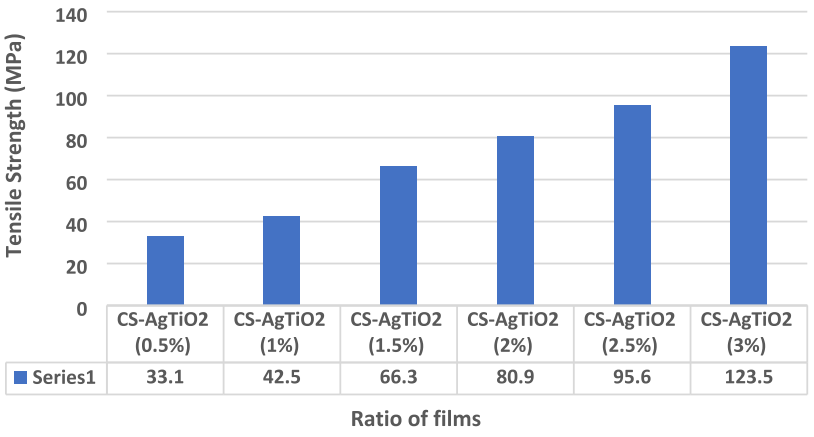

Figure 10. Tensile strength of Cs-$AgTiO_2$ at different concentrations.

Table 4

sample code	control	replica	dead shrimps after 24 h	LC_{50} (μg/mL)
Cs-$AgTiO_2$ (0.5%)				
1000	10	3	11	
100	10	3	4	218.039
10	10	3	2	
Cs-$AgTiO_2$ (01%)				
1000	10	3	14	
100	10	3	5	226.013
10	10	3	3	
Cs-$AgTiO_2$ (1.5%)				
1000	10	3	18	
100	10	3	7	232.014
10	10	3	2	
Cs-$AgTiO_2$ (02%)				
1000	10	3	26	
100	10	3	8	244.021
10	10	3	2	
Cs-$AgTiO_2$ (2.5%)				
1000	10	3	29	
100	10	3	6	274.032
10	10	3	2	
Cs-$AgTiO_2$ (03%)				
1000	10	3	33	
100	10	3	7	314.012
10	10	3	3	

$AgTiO_2$-NPs (3%) exhibited excellent nematicidal potential (64.20 ± 1.23 μg/mL), which could make these films a suitable novel material to control nematode spread in food. This research could offer different perspectives on how to create nanocomposite materials, improve their antibacterial properties, and more.

4. MATERIALS AND METHODS

Chitosan (C3646 degree of deacetylation ca 75%, viscosity > 200 cP), HCl (hydrochloric acid), ethanol 97%, TEOS 98% (tetraethyl orthosilicate), formic Acid (Mw: 46.03), PVA (Mw: 146,000−186,000), poly(vinyl alcohol), peptone ((1249-500), sodium chloride (58.344 g/mol), calcium chloride (Mw: 110.98 g/mol), distilled water, cholesterol (Mw: 386.65 g/mol), $MgSO_4$ (Mw: 246.47 g/mol)), KPO_4 buffer, 96-well plates, nutrient growth medium (NGM) plates, and chloroform were obtained from Sigma Aldrich. *C. elegans* (Strain N2), and *E. coli* (OP5O) were purchased from the *C. elegans* Genetic Center, University of Minusita. *Candida albicans* (ATCC 10231) was purchased from National Chemical Laboratory (NCL) in Pune, Maharashtra, India. All strains were used as received.

4.1. Preparation of the Chitosan Membrane (Cs-$AgTiO_2$). Silver-doped titanium dioxide was prepared by the reported method.[39] Cs was dissolved in a formic acid solution (02% v/v) at room temperature. PVA was dissolved in distilled water (10 mL). Both Cs and PVA solutions were mixed while stirring. Later on, different concentrations of $AgTiO_2$ (0.005 g, 0.01 g, 0.015, 0.02, 0.025, and 0.03%) were added to the above-mentioned solution. TEOS was hydrolyzed and added to the above-mentioned solution and stirred for 1 h at 40 °C. After 1 h, the resultant solutions were poured into Petri dishes for drying, which were placed in a dust-free environment. After drying, the films were stored for further analysis (Figure 11).

4.2. Characterization. *4.2.1. Fourier Transform Infrared Spectroscopy (FTIR).* Infrared spectra of the chitosan composite were recorded between 400 and 4000 cm^{-1} by using a 640 IR spectrophotometer for the structural and functional group determination. The potassium bromide (KBr) pellet method was applied for FTIR examination.

4.2.2. X-ray Diffraction Analysis (XRD). The crystalline phase was investigated through the use of an X-ray diffractometer (JDX 3523, JEOL, Japan), which was set to Cu K α radiation (λ = 1.5418) and operated throughout the range of 2 between 0 and 160. Using XPERT high-score software, the phase was identified by comparing with standard cards.

4.2.3. Scanning Electron Microscopy (SEM). Scanning electron microscopy, JSM 5910, JEOL, Japan, was used to analyze the sample's morphology, which was operated inside a high vacuum at 30kv, and the magnification power and maximum resolution are 300,000X and 2.3 nm, respectively.

4.2.4. Transmission Electron Microscopy (TEM). Transmission electron microscopy (TEM, JEM-2100 Japan) was used to analyze the samples's nature. For TEM images, the sample was mounted on a carbon-coated copper grid.

4.2.5. Tensile Strength. The tensile strength was measured on a TTM computer-based tensile tester with 30 mm spacing at a tension of 5N.

4.2.6. Antibacterial Activity. The agar well diffusion technique was used to evaluate the antibacterial activity of the synthesized films against Gram-negative bacteria. GNB (*E. coli*) were employed in this investigation. The sterilized Petri plates were then filled with the overnight bacterial culture that had been placed over freshly made, sterilized agar medium. The

https://doi.org/10.1021/acsomega.3c00068
ACS Omega 2023, 8, 19341−19350

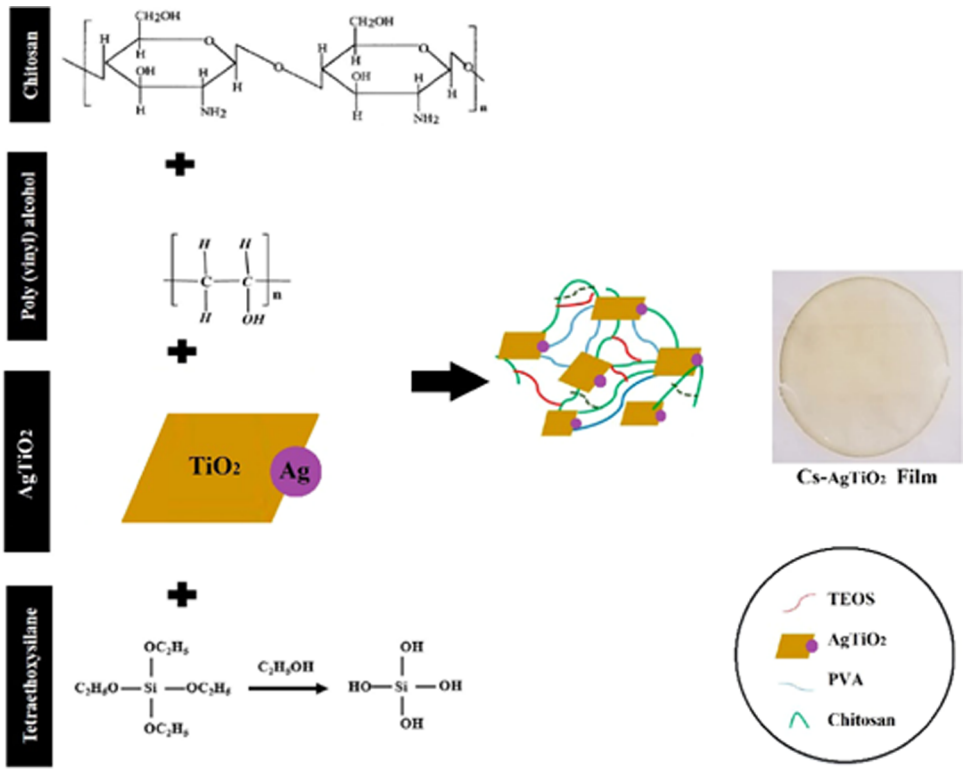

Figure 11. Schematic diagram and image of Cs-$AgTiO_2$ films.

culture was then allowed to harden at room temperature in a laminar air flow hood (YJ Clean Work Station).

Each plate was prepared by using a sterile micropipette tip to bore 5 mm-diameter wells and then a sterilized needle to remove the agar plug. An ultrasonic dispersion containing 5 mg/5 mL synthesized films was produced using DMSO, while 30 mg/mL of each suspension was added to each well before being incubated at 37 °C overnight. The zone of inhibition surrounding each well was measured in millimeters to determine the activity of the solutions after 24 h.

4.2.7. Antifungal Activity. The antifungal culture of the synthesized films versus *C. Albicans* isolates was assessed using a broth microdilution test according to the Laboratory & Clinical Standard Institute requirements. The synthesized Cs-$AgTiO_2$ solution was prepared by using 1% DMSO at an initial concentration of 1000 μg/mL, and then, Cs-$AgTiO_2$ was evaluated at concentrations between 250 and 0.125 μg/mL. All of the plates that were streaked using *C. Albicans* treated and isolated with synthesized films had been incubated at 37 °C for 24 h, and the minimum inhibitory concentrations (MICs) were visually recorded. 1% DMSO and fluconazole were used as negative and positive controls, respectively.

In order to determine the minimum fungicidal concentration (MFC), all wells exhibiting no growth were subsequently subcultured using Sabouraud dextrose agar (SDA) plates and afterward incubated at 37 °C for 24 h. MFC was defined as the lowest concentration at which no growth occurred on plates.

4.2.8. Antinematode Activity. The NGM plates were used to grow *C. elegans* (strain N2) with *E. coli* (OP50) as a source of food. The nematicidal activity was characterized using an uncontaminated 24/96-well microtiter plate (flat-bottom wells, polystyrene, Corning, New York, NY). The synthesized films were dissolved in solvents (DMSO) at concentrations of 80 μg/mL. S medium was then supplied directly toward the wells. 10 μL of the overnight culture of *E. coli* in the laboratory, suspended in S medium, at 5X concentration, was introduced into the wells. Wells were treated with the addition of 10−100 *C. elegans*. At 20 °C, the plates were incubated. After 24 h of incubation, a microscope was used to measure *C. elegans*. (Nikon Eclipse TS-100).

AUTHOR INFORMATION

Corresponding Author

Wajid Rehman − *Department of Chemistry, Hazara University, Mansehra 21120, Pakistan;* orcid.org/0000-0003-0128-0377; Email: sono_waj@yahoo.com

Authors

Muhammad Usman Khan − *Department of Chemistry, Hazara University, Mansehra 21120, Pakistan*

Saira Bibi − *Department of Chemistry, Hazara University, Mansehra 21120, Pakistan*

Mohammed M. Alanazi − *Department of Pharmaceutical Chemistry, College of Pharmacy, King Saud University, Riyadh 11451, Saudi Arabia*

Ashwag S. Alanazi − *Department of Pharmaceutical Sciences, College of Pharmacy, Princess Nourah bint Abdulrahman University, Riyadh 11671, Saudi Arabia*

Liaqat Rasheed − *Department of Chemistry, Hazara University, Mansehra 21120, Pakistan*

Shoaib Khan − *Department of Chemistry, Hazara University, Mansehra 21120, Pakistan*

Syed Umar Tariq Gillani − *Department of Chemistry, Hazara University, Mansehra 21120, Pakistan*

Arslan Tauqeer − *Department of Chemistry, Hazara University, Mansehra 21120, Pakistan*

Complete contact information is available at: https://pubs.acs.org/10.1021/acsomega.3c00068

https://doi.org/10.1021/acsomega.3c00068
ACS Omega 2023, 8, 19341−19350

Notes

The authors declare no competing financial interest.

■ ACKNOWLEDGMENTS

The authors extend their appreciation to the Researchers Supporting Project number (RSPD2023R628), King Saud University, Riyadh, Saudi Arabia for funding this research. The authors also extend their appreciation to Princess Nourah bint Abdulrahman University Researchers Supporting Project number (PNURSP2023R342), Princess Nourah bint Abdulrahman University, Riyadh, Saudi Arabia for funding this research.

■ ABBREVIATIONS

DMSOdimethyl sulfoxide; MFCminimum fungicidal concentration; MICsminimum inhibitory concentrations; NGMnematode growth media; TEOStetraethyl orthosilicate; SEMscanning electron microscopy; XRDX-ray diffraction analysis; FTIRFourier transform infrared spectroscopy; PVApoly(vinyl alcohol); DNAdeoxyribonucleic acid; $AgTiO_2$silver-doped titanium dioxide; GNBGram-negative bacteria; GPBGram-positive bacteria; Cschitosan; NGMnutrient growth media; SDASabouraud dextrose agar

■ REFERENCES

(1) Yu, Z.; Li, B.; Chu, J.; Zhang, P. Silica in situ enhanced PVA/chitosan biodegradable films for food packages. *Carbohydr. Polym.* **2018**, *184*, 214−220.
(2) Priyadarshi, R.; Rhim, J. W. Chitosan-based biodegradable functional films for food packaging applications. *Innovative Food Sci. Emerging Technol.* **2020**, *62*, No. 102346.
(3) US EPA. *Municipal Solid Waste Generation, Recycling, and Disposal in the United States: Facts and Figures for 2012*; US Environmental Protection Agency, 2014; pp 1−13.
(4) Breda, C. A.; Morgado, D. L.; Assis, O. B. G.; Duarte, M. C. T. Processing and characterization of chitosan films with incorporation of ethanolic extract from "pequi" peels. *Macromol. Res.* **2017**, *25*, 1049−1056.
(5) Mir, S. A.; Dar, B. N.; Wani, A. A.; Shah, M. A. Effect of plant extracts on the techno-functional properties of biodegradable packaging films. *Trends Food Sci. Technol.* **2018**, *80*, 141−154.
(6) Baygar, T. Bioactivity potentials of biodegradable chitosan/gelatin film forming solutions combined with monoterpenoid compounds. *J. Polym. Environ.* **2019**, *27*, 1686−1692.
(7) Kösemen, A.; Kösemen, Z. A.; Canimkubey, B.; Erkovan, M.; Başarir, F.; San, S. E.; Örnek, O.; Tunç, A. V. Fe doped TiO2 thin film as electron selective layer for inverted solar cells. *Sol. Energy* **2016**, *132*, 511−517.
(8) Morkoç, H.; Ozgür, U. *Zinc Oxide: Fundamentals, Materials and Device Technology*; Wiley-VCH: Weinheim, Germany, 2009.
(9) Jayabharathi, J.; Karunakaran, C.; Kalaiarasi, V.; Ramanathan, P. Nano ZnO, Cu-doped ZnO, and Ag-doped ZnO assisted generation of light from imidazole. *J. Photochem. Photobiol., A* **2014**, *295*, 1−10.
(10) Elsellami, L.; Dappozze, F.; Houas, A.; Guillard, C. Effect of Ag+ reduction on the photocatalytic activity of Ag-doped TiO_2. *Superlattices Microstruct.* **2017**, *109*, 511−518.
(11) Krejčíková, S.; Matějová, L.; Kočí, K.; Obalová, L.; Matěj, Z.; Čapek, L.; Šolcová, L. Preparation and characterization of Ag-doped crystalline titania for photocatalysis applications. *Appl. Catal., B* **2012**, *111-112*, 119−125.
(12) Ubonchonlakate, K.; Sikong, L.; Saito, F. Photocatalytic disinfection of P.aeruginosa bacterial Ag-doped TiO2 film. *Procedia Eng.* **2012**, *32*, 656−662.
(13) Hastir, A.; Kohli, N.; Singh, R. C. Ag doped ZnO nanowires as highly sensitive ethanol gas sensor. *Mater. Today: Proc.* **2017**, *4*, 9476−9480.
(14) Jakob, M.; Levanon, H.; Kamat, P. V. Charge distribution between UV-irradiated TiO2 and gold nanoparticles: determination of the shift in the Fermi level. *Nano Lett.* **2003**, *3*, 353−358.
(15) Jawaid, M.; Khalil, H. P. S. A. Cellulosic/synthetic fiber reinforced polymer hybrid composites: A review. *Carbohydr. Polym.* **2011**, *86*, 1−18.
(16) Liu, Y. L.; Chen, W. H.; Chang, Y. H. Preparation and properties of chitosan/carbon nanotube nanocomposites using poly (styrene sulfonic acid)-modified CNTs. *Carbohydr. Polym.* **2009**, *76*, 232−238.
(17) Sionkowska, A. Current research on the blends of natural and synthetic polymers as new biomaterials: Review. *Prog. Polym. Sci.* **2011**, *36*, 1254−1276.
(18) Wang, Y.; Wei, W.; Liu, X.; Zeng, X. Carbon nanotube/chitosan/gold nanoparticles-based glucose biosensor prepared by a layer-by-layer technique. *Mater. Sci. Eng., C* **2009**, *29*, 50−54.
(19) Islam, A.; Yasin, T.; Bano, I.; Riaz, M. Controlled release of aspirin from pH-sensitive chitosan/poly (vinyl alcohol) hydrogel. *J. Appl. Polym. Sci.* **2012**, *124*, 4184−4192.
(20) Zhai, M.; Zhao, L.; Yoshii, F.; Kume, T. Study on antibacterial starch/chitosan blend film formed under the action of irradiation. *Carbohydr. Polym.* **2004**, *57*, 83−88.
(21) Chen, X.; Mao, S. S. Titanium Dioxide Nanomaterials: Synthesis, Properties, Modifications, and Applications. *Chem. Rev.* **2007**, *107*, 2891−2959.
(22) Islam, A.; Raiz, M.; Yasin. Structural and viscoelastic properties of chitosan-based hydrogel and its drug delivery application. *Int. J. Biol. Macromol.* **2013**, *59*, 119−124.
(23) Jamnongkan, T.; Wattanakornsiri, A.; Pansila, P. P.; Migliaresi, C.; Kaewpirom, S. Effect of Poly(vinyl alcohol)/Chitosan Ratio on Electrospun-nanofiber Morphologies. *Adv. Mater. Res.* **2012**, *463−464*, 734−738.
(24) Sarteep, Z.; Pirbazari, A. E.; Aroon, M. A. Silver doped TiO2 nanoparticles: preparation, characterization and efficient degradation of 2, 4-dichlorophenol under visible light. *J. Water Environ. Nanotechnol.* **2016**, *1*, 135−2016.
(25) Wang, Y.; Ma, X.; Wen, Y.; Xing, Y.; Zhang, Z.; Yang, H. Direct electrochemistry and bioelectrocatalysis of horseradish peroxidase based on gold nano-seeds dotted TiO_2 nanocomposite. *Biosens. Bioelectron.* **2010**, *25*, 2442−2446.
(26) Lee, J.; Bagheri, B.; Kao, H. A. A Cyber-Physical Systems architecture for Industry 4.0-based manufacturing systems. *Manuf. Lett.* **2015**, *3*, 18−23.
(27) Kumar, M. S. C.; Selvam, V.; Vadivel, M. Synthesis and characterization of silane-modified iron (iii) oxide nanoparticles reinforced chitosan nanocomposites. *Int. J. Eng. Sci. Technol.* **2012**, *2*, 1258−1263.
(28) Pham, N. D.; Thao, N. H.; Luan, V. H.; Hoang, H. A.; Sagadevan, S.; Ngo, M. T.; Duong, N. N. H.; Le, M. V. Photocatalytic Disinfection of *E. coli* Using Silver-Doped TiO_2 Coated on Cylindrical Cordierite Honeycomb Monolith Photoreactor Under Artificial Sunlight Irradiation. *Top. Catal.* **2022**, *66*, 75−88.
(29) Munir, T.; Sharif, M.; Ali, H.; Kashif, M.; Sohail, A.; Sabir, N.; Amin, N.; Mahmood, A.; Ahmed, N. Impact of silver dopant on structural and optical properties of TiO2 nanoparticles. *Dig. J. Nanomater. Biostructures* **2019**, *14*, 279−284.
(30) Zhang, D. Y.; Liu, J.; Shi, Y. S.; Wang, Y.; Liu, H. F.; Hu, Q. L.; Su, L.; Zhu, J. Antifouling polyimide membrane with surface-bound silver particles. *J. Membr. Sci.* **2016**, *516*, 83−93.
(31) Habib, Z.; Khan, S. J.; Ahmad, N. M.; Shahzad, H. M. A.; Jamal, Y.; Hashmi, I. Anti-bacterial Behavior of Surface Modified Composite Polyamide Nanofiltration (NF) Membrane by Immobilizing Ag doped TiO_2 Nanoparticles. *Environ. Technol.* **2019**, 3657−3669.
(32) Kawahara, K.; Tsuruda, K.; Morishita, M.; Uchida, M. Antibacterial effect of silver-zeolite on oral bacteria under anaerobic conditions. *Dent. Mater. J.* **2000**, *16*, 452−455.
(33) Gupta, K.; Singh, R. P.; Pandey, A.; Pandey, A. Photocatalytic antibacterial performance of TiO2 and Ag-doped TiO_2 against *S. aureus*. *P. aeruginosa* and *E. coli*. *Bilstein J. Nanotechnol.* **2013**, *4*, 345−351.

https://doi.org/10.1021/acsomega.3c00068
ACS Omega 2023, 8, 19341−19350

(34) Shende, P.; Oza, B.; Guad, R. S. Silver-doped titanium dioxide nanoparticles encapsulated in chitosan−PVA film for synergistic antimicrobial activity. *Int. J. Polym. Mater. Polym. Biomater.* **2018**, *67*, 1080−1086.
(35) Waly, G. H. Effect of incorporating undoped or silver-doped photocatalytic titanium dioxide on the antifungal effect and dynamic viscoelastic properties of long-term acrylic denture liners. *Future Dent. J.* **2018**, *4*, 8−15.
(36) Saddiqi, H. A.; Jabbar, A.; Sarwar, M.; Iqbal, Z.; Ghulam, M.; Nisa, M.; Shahzad, A. Small ruminant resistance against gastrointestinal nematodes: a case of Haemonchus contortus. *Parasitol. Res.* **2011**, *109*, 1483−1500.
(37) Gonzalez-Moragas, L.; Roig, A.; Laromaine, A. C. elegans as a tool for in vivo nanoparticle assessment. *Adv. Colloid Interface Sci.* **2015**, *219*, 10−26.
(38) Khalid, L. K. Modification, Characterization and Evaluation of Anti-Microbial Property of Ag-TiO2 nanoparticles coated Traditional Leather. *Bayero J. Pure Appl. Sci. 13* 53 59.
(39) Petica, A.; Floreab, A.; Gaidaua, C.; Balanc, D.; Anicai, L. Synthesis and characterization of silver-titania nanocomposites prepared by electrochemical method with enhanced photocatalytic characteristics, antifungal, and antimicrobial activity. *J. Mater. Res. Technol.* **2019**, *8*, 41−53.

https://doi.org/10.1021/acsomega.3c00068
ACS Omega 2023, 8, 19341−19350